

Suppression of Spin Pumping Between $\text{Ni}_{80}\text{Fe}_{20}$ and Cu by a Graphene Interlayer

Will Gannett, Mark W. Keller,* Hans T. Nembach, Thomas J. Silva, and Ann Chiaramonti Debay
National Institute of Standards and Technology, Boulder, CO 80305 [†]

We compare ferromagnetic resonance measurements of Permalloy $\text{Ni}_{80}\text{Fe}_{20}$ (Py) films sputtered onto Cu(111) films with and without a graphene (Gr) interlayer grown by chemical vapor deposition before Py deposition. A two-angle sputtering method ensured that neither Gr nor Py was degraded by the sample preparation process. We find the expected damping enhancement from spin pumping for the Py/Cu case and no detectable enhancement for the Py/Gr/Cu case. Since damping is sensitive to effects other than spin pumping, we used magnetometry to verify that differences in Py magnetostatic properties are not responsible for the difference in damping. We attribute the suppression of spin pumping in Py/Gr/Cu to the large contact resistance of the Gr/Cu interface.

I. INTRODUCTION

The complex interactions between magnetization dynamics in a ferromagnet and the flow of charge and spin currents is a topic that combines rich physics and relevance to technological applications. These interactions are often divided into two types that are reciprocal manifestations of the same microscopic process [1]. *Spin transfer* refers to the torque exerted on the magnetization by a flow of spins (with or without an associated flow of charge). *Spin pumping* refers to the flow of spins generated by a precessing magnetization. The first effect enables control of magnetization through an applied current [2], rather than an applied magnetic field, and is crucial to realizing a scalable magnetic random access memory [3]. The second effect is most often encountered as an enhanced damping of magnetization dynamics when a thin ferromagnetic (FM) film is in contact with a nonmagnetic (NM) material that absorbs the spin current [4, 5]. This loss of angular momentum adds to the intrinsic dissipation of the FM material, causing an enhancement of the Gilbert damping parameter α . The effect on damping can be quite large ($\gtrsim 2\times$) for ultrathin ($\lesssim 10\text{ nm}$) FM films and has been observed for many FM/NM combinations [5–11].

Brataas *et al.* [1] have reviewed the phenomenology and the quantitative theory of spin transfer and spin pumping. When considering the effect of spin pumping on FM damping, it is useful to identify two limiting cases. If the FM is in contact with a material that strongly scatters or absorbs the pumped spin current, α is increased substantially. In contrast, if the NM does not act as a spin sink, then pumped spins will accumulate in the NM and drive a diffusive spin current back toward the FM that cancels the spin pumping current in steady state. In this “spin battery” limit, there is no effect on α . For a general case, the change in damping for a FM film of thickness d_{FM} is determined by an effective spin conduc-

tance per unit area, G_{eff} (units of $\Omega^{-1} \cdot \text{m}^{-2}$), according to

$$\Delta\alpha_{\text{sp}} = \frac{|\gamma|\hbar^2}{2e^2M_s d_{\text{FM}}} G_{\text{eff}}, \quad (1)$$

where γ is the gyromagnetic ratio, e is the electron charge, \hbar is the reduced Planck constant, and M_s is the saturation magnetization of the FM. The conductance G_{eff} includes contributions from the FM/NM interface and from spin diffusion in the NM material (see Appendix A).

Graphene (Gr) is expected to be a useful material for spintronics because its high carrier mobility and low spin scattering should allow propagation of spin currents over long distances ($\gg 1\text{ }\mu\text{m}$) at room temperature. Spin coherence lengths of about $1\text{ }\mu\text{m}$ have been demonstrated by injecting spin-polarized charge current from FM contacts into a Gr channel [12]. The main challenge facing these devices is the limited efficiency for injecting spin-polarized carriers from the metallic FM into a channel having much lower electrical conductivity. Even with tunnel barriers between the FM and the Gr designed to minimize this effect, the efficiency is only about 30% [12]. Since spin pumping involves only spins and not charges flowing between the FM and NM materials, it provides a way to inject spin current from FM metals into Gr that is not limited by the mismatch in electrical conductivity.

This paper compares ferromagnetic resonance (FMR) measurements of Permalloy $\text{Ni}_{80}\text{Fe}_{20}$ (Py) films with nominal thicknesses between 8 nm and 45 nm sputtered onto Cu(111) films with and without a Gr interlayer grown by chemical vapor deposition (CVD) before Py deposition. The Py films were deposited using a two-step process (see section III A) that avoids damage to the Gr and yields high quality Py. The FMR results show the expected damping enhancement for the Py/Cu case but no enhancement for the Py/Gr/Cu case. This unexpectedly strong effect on spin transport by a monolayer of material with weak intrinsic spin scattering requires careful validation. Since FM damping is sensitive to effects other than spin pumping, much of the paper is concerned with ensuring that neither Gr nor Py is significantly degraded

* mark.keller@nist.gov

[†] Contribution of the National Institute of Standards and Technology; not subject to copyright in the United States.

by the sample preparation process. In particular, we use a novel two-angle sputtering geometry, we verify the Gr quality using Raman spectroscopy, we use magnetometry to measure the moment and coercivity of each sample, and we examine the Py morphology using transmission electron microscopy.

Previous studies have shown evidence for spin pumping from Py into Gr [13, 14], but the use of only a single thickness of Py and the lack of magnetometry or other characterization of the Py itself limits the conclusions that can be drawn from the observed effects. We discuss these limitations in detail, drawing on our results and on other recently published work [15]. Finally, we attribute the suppression of spin pumping in Py/Gr/Cu to the large contact resistance of the Gr/Cu interface [16].

II. FMR MEASUREMENT OF SPIN PUMPING

For FMR measurements, samples were placed on a coplanar waveguide with a center conductor width of $100\ \mu\text{m}$, and the scattering parameter S_{21} was measured using a vector network analyzer. The static magnetic field H was applied perpendicular to the sample plane and was large enough to saturate the magnetization, suppressing the 2-magnon scattering contribution to the FMR linewidth [17]. For each excitation frequency f , fitting the real and imaginary parts of $S_{21}(H)$ yields the resonance field $H_{\text{res}}(f)$ and the field-swept linewidth $\Delta H(f)$. Details of the measurement and data analysis techniques are described in [18].

The FMR resonance field and linewidth as a function of excitation frequency are given by

$$H_{\text{res}}(f) = \frac{2\pi f}{|\gamma|\mu_0} + M_{\text{eff}} \quad (2)$$

$$\Delta H(f) = \frac{4\pi f\alpha}{|\gamma|\mu_0} + \Delta H_0, \quad (3)$$

where μ_0 is the magnetic constant, $M_{\text{eff}} = M_s - H_k^\perp$ is the effective magnetization including a perpendicular anisotropy field H_k^\perp , and ΔH_0 is the broadening due to inhomogeneity in the local resonance field across the sample [18]. A linear fit to Eq. 2 gives values for γ and M_{eff} , and a linear fit to Eq. 3 gives values for α and ΔH_0 [18]. Results for all four fitted parameters are given in Appendix B.

Figure 1 shows α as a function of d_{FM} for two sets of Py samples. The Py/Cu samples clearly show an increase in α as d_{FM} decreases, as seen previously [8] and as expected from Eq. 1, while the Py/Gr/Cu samples show no significant change in α . As shown in the next section, the Py in the two sets of samples has very similar magnetic and morphological properties, so this result is strong evidence for suppression of spin pumping between Py and Cu due to the Gr interlayer.

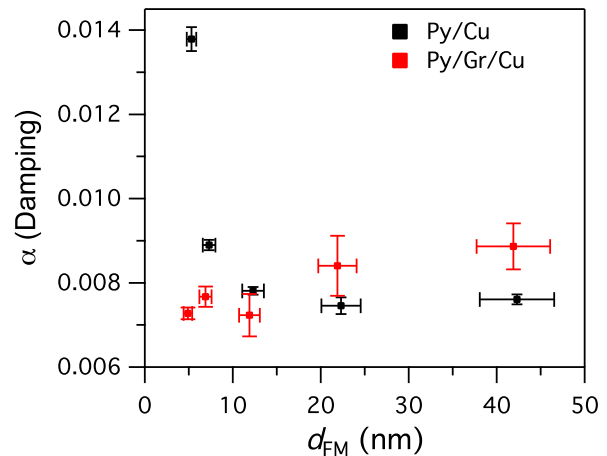


FIG. 1. Damping vs. thickness for Py deposited on bare Cu (Py/Cu) and on Cu covered by CVD Gr (Py/Gr/Cu). Vertical error bars show the uncertainty from the linear fits to Eq. 3. The larger uncertainty in α for the thicker Gr samples is due to a larger scatter in $\Delta H(f)$ for these samples. Horizontal error bars reflect an estimated 10% uncertainty in deposition rate.

III. SAMPLE PREPARATION AND CHARACTERIZATION

A. Motivation for Two-angle Sputtering

Damage to Gr during magnetron sputtering of Ti and Al has been studied using Gr flakes exfoliated onto Si substrates [19]. This work considered several types of bombardment present in sputtering (electrons, photons, depositing atoms, and inert gas atoms) and concluded that damage is primarily due to inert gas atoms, which can be reflected from the target as neutral atoms with sufficient energy to displace C atoms from Gr. Detailed simulations [20] of sputtering a Cu target in Ar gas show, for a typical discharge voltage of 400 V, that Cu atoms leave the target with an average energy of about 10 eV, while Ar neutrals are reflected with an average energy of about 45 eV. For comparison, the displacement threshold for Ar striking Gr at normal incidence is 33 eV [21, 22]. Increasing the gas pressure or target-to-substrate distance reduces the flux of both Ar neutrals and depositing atoms, but since the more energetic Ar atoms have a longer mean free path than the depositing atoms [20], the deposition rate is strongly suppressed before the Gr is protected from Ar impacts. Since the displacement threshold increases away from normal incidence [21, 22], damage can be avoided by orienting the substrate perpendicular to the target, as seen in Fig. 2 with $\theta = 90^\circ$. The tradeoff between deposition rate and Gr damage for orientations near perpendicular was quantified for Ti and Al in [19].

For many magnetic materials, including Py, bombardment of the substrate is important in promoting growth

of thin films that are homogeneous and have properties such as M_s and α that are close to bulk values. Thus a substrate orientation perpendicular to the target is undesirable in terms of film quality as well as deposition rate. For this reason, we chose to deposit Py at two separate orientations, as shown in Fig. 2. The first deposition, 5 nm at $\theta = 90^\circ$, covers the Gr with a Py film of low quality but does not damage the Gr, and this Py layer protects the Gr from damage during the second deposition, at $\theta = 30^\circ$, that yields high quality Py. The two depositions were done without breaking vacuum by use of an angled sample holder (see Methods section). Importantly, transmission electron microscopy (see Section III C and Fig. 5) shows the final Py film to be a single, homogeneous layer rather than two distinct layers. We attribute the lack of a morphological boundary between the two layers to bombardment during the second deposition. The sum of the first and second deposition thicknesses is the nominal Py thickness, d_0 .

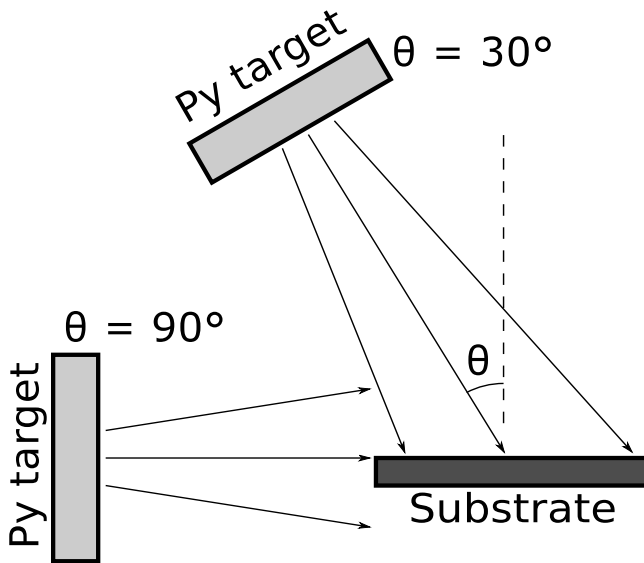


FIG. 2. Schematic of deposition at two angles θ relative to substrate normal direction (not to scale). The Py target is shown in different positions for clarity, but in practice θ was changed by tilting the substrate.

B. Gr Properties

We used Raman spectroscopy to measure Gr damage as follows. The Raman spectrum of pristine Gr has two characteristic peaks, named G and 2D, and defects allow an additional scattering mechanism that adds a feature named the D peak [23]. The ratio of the peak intensities for the D and G features, I_D/I_G , can be used to estimate the number of point defects per unit area [24].

For our as-grown Gr on Cu, we found a baseline value of $I_D/I_G = 0.11 \pm 0.03$, which implies one defect every $(1300 \pm 350) \text{ nm}^2$. We deposited 5 nm to 35 nm of

Py at $\theta = 90^\circ$ on several samples and found no change in I_D/I_G , demonstrating that sputtering in this geometry does not damage Gr. The fact that Gr Raman peaks could be measured through these films indicates the Py deposited at $\theta = 90^\circ$ was highly transparent, consistent with the fact that these samples still showed some Cu color after deposition. In contrast, Py deposited at $\theta = 30^\circ$ did not show any Gr Raman peaks for thickness $\geq 2 \text{ nm}$ and had a color similar to that of high quality Ni films. A short deposition at $\theta = 30^\circ$, lasting $\approx 2 \text{ s}$ and giving $\approx 0.2 \text{ nm}$, allowed us to measure Gr Raman peaks with $I_D/I_G = 1.7$, corresponding to one defect every 100 nm^2 . This confirms that Gr is readily damaged by sputtering in this geometry, with a damage rate of roughly $0.005 \text{ nm}^{-2} \cdot \text{s}^{-1}$. In fact, this rate is close to the flux of Ar neutrals expected from the simulations in [20] (see Appendix C).

We estimated the potential damage to Gr covered by Py using the Stopping and Range of Ions in Matter (SRIM) Monte Carlo simulation [25]. Since the substrate in our case is located 23 cm from the target, only Ar neutrals reflected nearly perpendicular to the target will reach the substrate, with a maximum energy of $\approx 70 \text{ eV}$ for a 430 V discharge [20]. For 10^7 Ar ions at 70 eV and normal incidence, SRIM predicts no transmission for 5 nm of Py with its nominal density of 8.7 g/cm^3 . Adjusting parameters to reflect the fact that Py deposited at $\theta = 90^\circ$ is different from nominal, *e.g.*, using a thickness of 2 nm and nominal density, or a thickness of 5 nm and a density of 3 g/cm^3 , yielded a transmission probability of less than 1 in 10^7 . Combining this with the Ar neutral flux estimated in Appendix C shows that damage due to Ar penetration through the $\theta = 90^\circ$ Py film is expected to be negligible.

C. Py properties

In addition to FMR measurements, we used vibrating sample magnetometry (VSM) to measure Py magnetostatic properties of the same samples presented in Fig. 1. We also used transmission electron microscopy (TEM) to characterize Py morphology for separate, similarly prepared samples.

For a homogeneous FM film with magnetization M_s and thickness d_0 , the moment per unit area is $\mu_0 M_s d_0$. The total magnetic moment measured by VSM, divided by the area of each sample, is plotted vs. nominal Py thickness in Fig. 3. From the slopes of the linear fits in Fig 3, we find $\mu_0 M_s = (1.1 \pm 0.1) \text{ T}$ for both Py/Cu and Py/Gr/Cu samples. The nonzero intercepts of the fits imply the actual thickness of the films is $\approx 3 \text{ nm}$ less than the nominal thickness. This is not surprising, since the 5 nm of Py deposited at $\theta = 90^\circ$ is porous (see Section III B) and some of the Py deposited at $\theta = 30^\circ$ will fill the pores instead of adding to the overall film thickness. For the rest of this paper, we use the actual FM thickness d_{FM} obtained by subtracting the intercept

values from d_0 .

Given the actual FM thickness values, we can use M_{eff} measured by FMR to determine the perpendicular anisotropy of the Py as follows. Figure 4 shows plots of M_{eff} vs. $1/d_{\text{FM}}$ for the two-angle Py/Cu and Py/Gr/Cu samples, and for several samples deposited only at $\theta = 30^\circ$. The linear dependence for all samples is consistent with a constant interfacial anisotropy energy K_{int} , for which M_{eff} is given by

$$M_{\text{eff}} = M_s - \frac{2K_{\text{int}}}{\mu_0 M_s d_{\text{FM}}}.$$

Thus the intercept of each linear fit in Fig. 4 gives M_s and the slope gives K_{int} . We find $\mu_0 M_s = (1.01 \pm 0.02)$ T for both Py/Cu and Py/Gr/Cu samples, consistent with the value obtained from VSM data. The values of K_{int} , given in Table I, are quite similar for a given deposition method, but are noticeably larger for two-angle films than for single-angle films. Furthermore, our values are larger than the value of $K_{\text{int}} \approx 1 \times 10^{-4} \text{ J/m}^2$ reported for Py/Cu [26] and Py/air [27] interfaces. These differences are likely due to variations in how Py nucleates and grows on different substrates, for example polycrystalline Cu compared to our Cu(111), in addition to the different deposition geometries.

The coercive field measured by VSM is 0.5 mT for Py/Cu and 0.25 mT for Py/Gr/Cu. Although both values are somewhat larger than the ≈ 0.1 mT typically found for high-quality Py, similar values have been reported for Py deposited on Cu(111) single crystals [28]. Finally, a 40 nm Py/Cu film deposited at a single angle of $\theta = 30^\circ$ showed the same value of α (≈ 0.008) as the two-angle Py/Cu film with 5 nm at $\theta = 90^\circ$ and 40 nm at $\theta = 30^\circ$, indicating that the intrinsic damping of the Permalloy is not affected by two-angle deposition.

Overall, these results show that whatever effects Gr may have on the film growth process, for our two-angle method it has little or no effect on the Py magnetic properties.

We prepared samples for cross-sectional TEM imaging using a standard lift-out technique in a focused ion beam microscope [29]. Following a thinning step using 5 kV Ga^+ ions, we performed a final cleaning and thinning using 900 eV Ar^+ ions.

An image of a two-angle Py film deposited on Gr/Cu, 10 nm at $\theta = 90^\circ$ and 10 nm at $\theta = 30^\circ$, is shown in Fig. 5. While the film is quite rough, it is continuous and, importantly, shows neither internal voids nor an apparent boundary between the two Py layers. This suggests that

any holes in the first layer are filled in during the second deposition. The Py grains are fairly round and selected area diffraction patterns (not shown) indicate a modest (111) texture.

IV. DISCUSSION

Since our co-deposited Py/Cu and Py/Gr/Cu films have the same magnetization, similar perpendicular anisotropies, and nearly the same damping for films 15 nm and thicker, the dramatic difference in damping for thinner films (see Fig. 1) must be attributed to the Gr interlayer. We do not expect other effects such as surface oxidation and surface roughness to be substantially different between the two types of samples. This leads to the surprising conclusion that a single layer of C atoms can block the transfer of spins between two metals. Before offering an explanation for this effect, we first compare our results with other FMR measurements of Py films deposited on Gr.

In [30] and [14], Gr grown by CVD on Cu foils was transferred to insulating or semiconducting substrates and Py was deposited by thermal evaporation to give Py/substrate and Py/Gr/substrate samples. Only a single Py thickness, 14 nm, was used for all samples in these two studies. In [30], for samples where the Py covered the entire Gr area, the Py damping was 1.9 times larger when Gr was present. This was interpreted as evidence for strong spin scattering in Gr itself, which would be contrary to all expectations. However, M_{eff} was also different for these samples (30% lower with Gr present) which suggests the difference in damping could be due to differences in the Py itself rather than the presence of Gr. In [14], the same group made Py/Gr samples where the Gr extended $\approx 10 \mu\text{m}$ past two edges of the Py film. Damping for these samples was 1.1 times larger than for similar samples where the Py covered the entire Gr area. This small change in damping cannot be reliably attributed to spin pumping without further measurements to rule out changes in the Py. Unfortunately, no independent measurements of M_s or H_k^\perp were reported in [30] or [14]. Further evidence of the need for caution comes from a study of 14 nm thick Co films deposited by evaporation onto Gr/SiO₂ and SiO₂ substrates [15]. Careful characterization by FMR, magnetometry, magnetic force microscopy, and Kerr microscopy revealed such clear magnetic differences between the samples that the authors, commendably, declined to draw any conclusions about spin pumping into Gr.

In [13], Py and Pd were evaporated onto a Gr/SiO₂ substrate and patterned into stripes separated by about $1 \mu\text{m}$ of unpatterned Gr. When the Py was driven to precess by an 9.62 GHz magnetic field, a voltage was detected in the Pd stripe that behaved as expected if a spin current was pumped from the Py into the Gr channel and then generated an inverse spin Hall voltage after diffusing to the Pd. FMR measurements at this same frequency

	K_{int} (J/m ²)
Py/Cu, two-angle	$(6.6 \pm 0.6) \times 10^{-4}$
Py/Gr/Cu, two-angle	$(5.6 \pm 0.6) \times 10^{-4}$
Py/Cu, $\theta = 30^\circ$	$(3.8 \pm 0.3) \times 10^{-4}$
Py/Gr/Cu, $\theta = 30^\circ$	$(3.5 \pm 0.3) \times 10^{-4}$

TABLE I. Anisotropy energies from FMR measurements.

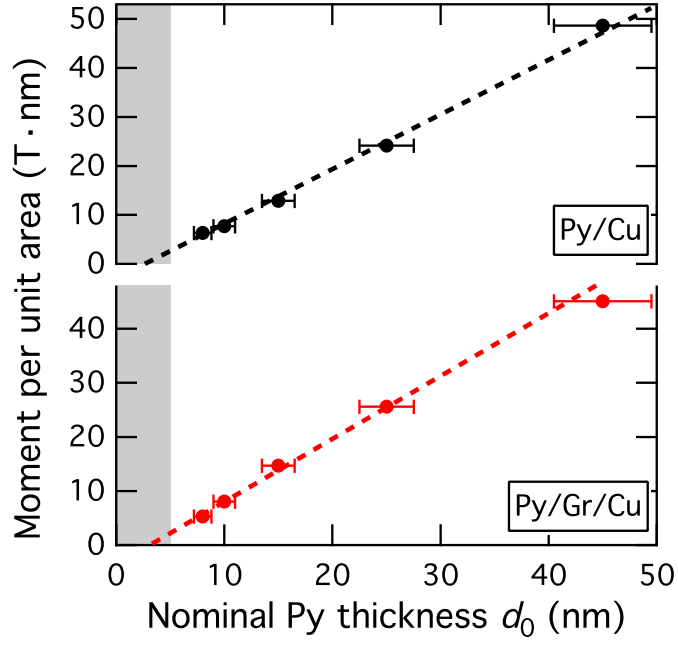


FIG. 3. Magnetic moment per unit area vs nominal Py thickness from VSM measurements. The gray shaded region indicates the initial 5 nm of Py deposited at glancing incidence, $\theta = 90^\circ$. The rest of the Py was deposited at $\theta = 30^\circ$. Horizontal error bars reflect an estimated 10% uncertainty in deposition rate, and the fits are weighted accordingly.

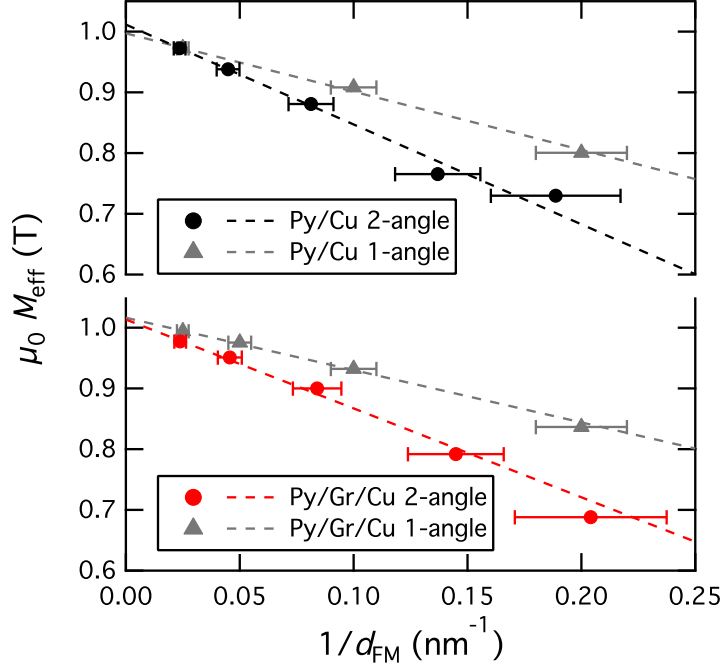


FIG. 4. M_{eff} vs. $1/d_{\text{FM}}$ with weighted linear fits for samples deposited at two angles and at a single angle ($\theta = 30^\circ$).

showed the linewidth for Py/Gr/SiO₂ was 0.5 mT larger than for Py/SiO₂, for 25 nm thick Py. This difference was attributed to spin pumping from Py to Gr, but since ΔH_0 was not measured the difference could equally be

due to differences in the Py itself. The fact that ΔH_0 for our 25 nm Py films differed by 0.9 mT, while α differed by only 1%, shows that FMR linewidth at a single frequency does not yield a reliable estimate for damping or

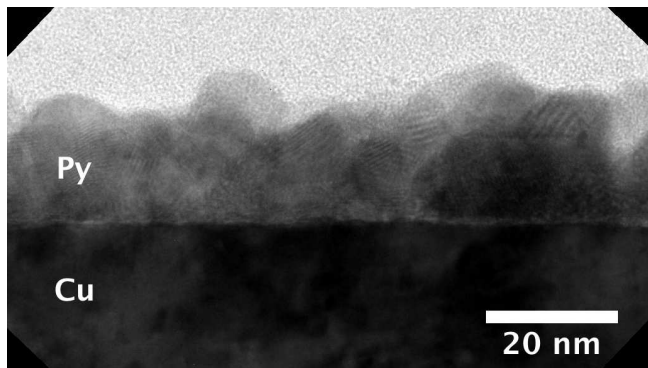


FIG. 5. TEM cross-section image of a Py/Gr/Cu sample with 10 nm deposited at $\theta = 90^\circ$ and 10 nm deposited at $\theta = 30^\circ$.

spin pumping.

The limitations of these previous experiments can be avoided by varying both FMR frequency and FM thickness over a wide range. The frequency range reveals what fraction of FMR linewidth is due to damping (α) as opposed to inhomogeneity (ΔH_0). The plot of α vs. d_{FM} allows a clear separation of the intrinsic and spin pumping contributions to α at each thickness.

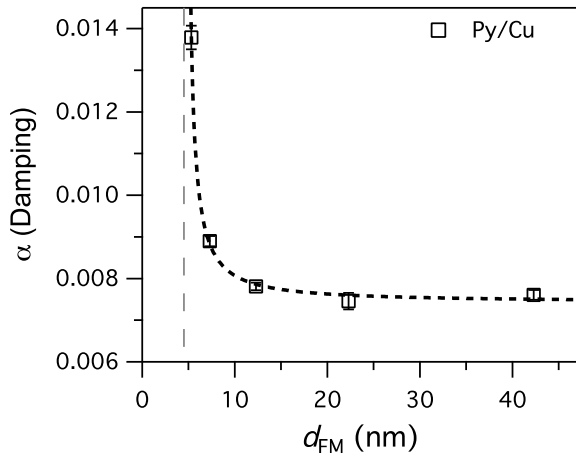


FIG. 6. Fit to damping vs. thickness for Py/Cu samples using Eq. 1.

For our Py/Cu samples, the spin pumping expression in Eq. 1 can be fit to the data shown in Fig. 1 and reproduced in Fig. 6. For this fit we used the value of M_s calculated from the data in Fig. 4. We also added an adjustable thickness t_d^{SP} , representing a Py “dead layer” that does not contribute to spin pumping. Finally, we added an adjustable intrinsic damping α_0 to account for non-zero damping at large thickness. The fit then yields $\alpha_0 = 0.0074 \pm 0.0001$, $G_{\text{eff}} = (8.6 \pm 1.6) \times 10^{13} \Omega^{-1} \cdot \text{m}^{-2}$, and $t_d^{\text{SP}} = 4.7 \pm 0.7 \text{ nm}$, and is shown by the dashed curve in Fig. 6. The uncertainty in t_d^{SP} is largely due to uncertainty in the thickness of the thinnest film.

As described in Appendix A, we use a model for G_{eff} that combines an interfacial spin mixing conductance $G_{\uparrow\downarrow}$ and an external conductance G_{ext} as resistors in series, i.e.,

$$\frac{1}{G_{\text{eff}}} \equiv \frac{1}{G_{\uparrow\downarrow}} + \frac{1}{G_{\text{ext}}}. \quad (4)$$

The interfacial contribution is of order $10^{15} \Omega^{-1} \cdot \text{m}^{-2}$ (see Appendix A), so G_{eff} in our case is dominated by G_{ext} and insensitive to the value of $G_{\uparrow\downarrow}$. We can therefore neglect $G_{\uparrow\downarrow}$ and, using the expression for G_{ext} given in Appendix A and a bulk conductivity for Cu of $\sigma = 5.8 \times 10^7 \Omega^{-1} \cdot \text{m}^{-1}$, we infer a spin diffusion length in Cu of $\lambda_s = 310 \pm 60 \text{ nm}$. This value is roughly consistent with the various room temperature values compiled in [31].

While we are unable to find prior measurements of spin pumping dead layers at Py/Cu interfaces, measurements on other FM/NM systems show much thinner dead layers, $\sim 1 \text{ nm}$ [32]. This could be due to differences in the Py/Gr interface due to our unusual deposition conditions. Additionally, our 1-D spin pumping model does not account for lateral sample inhomogeneity, such as that from roughness observed in Fig. 5, but the effect of in-plane spin currents on our parameters is unknown.

A likely explanation for the dramatic suppression of spin pumping by a single Gr layer is the electrical contact resistance between Gr and Cu. Measurements for several metals deposited on Gr gave a value of $1/G_c \approx 10^{-9} \Omega \cdot \text{m}^2$ for Cu and values of $\approx 2 \times 10^{-11} \Omega \cdot \text{m}^2$ for Ni, Ti, Pd, and Pt [16]. Adding this term to Eq. 4, we expect $G_{\text{eff}} \approx G_c \approx 10^9 \Omega^{-1} \cdot \text{m}^{-2}$ for Py/Gr/Cu, which is nearly 5 orders of magnitude smaller than G_{eff} for Py/Cu. Thus the Gr/Cu interface presents a large barrier to spin flow, reducing the net flow of spin current away from the Py to the point where even our thinnest films show no enhanced damping.

Even the lowest metal-Gr contact resistances are much larger than $1/G_{\uparrow\downarrow}$, which raises the question of whether spin pumping into Gr is possible under any conditions. Although the values of $G_{\uparrow\downarrow}$ and λ_s inferred in [13] depend entirely on a questionable value for $\Delta\alpha_{\text{sp}}$, the voltage detected at the Pd in those experiments is strong evidence that spins did flow from the Py to the Pd. Given this evidence, we believe it is likely that in our Py/Gr/Cu samples there is significant spin pumping into the Gr, but also a large spin accumulation because of the barrier at the Gr/Cu interface and therefore a large diffusion of spins back into the Py. A quantitative understanding of this situation, in which the same monolayer of C atoms participates in both the Py/Gr and the Gr/Cu interfaces, is a rich topic for further investigation.

V. CONCLUSION

In summary, we prepared Py/Cu and Py/Gr/Cu samples with varying Py thickness d_{FM} , using a two-angle sputtering method and carefully verifying that neither Gr

nor Py were degraded. We used FMR to measure damping α for both series of samples. The Py/Cu samples showed an increase in α with decreasing d_{FM} , as expected from spin pumping. Fitting the standard model of spin pumping showed G_{eff} was dominated by G_{ext} of the Cu rather than the interfacial conductance $G_{\uparrow\downarrow}$, which precludes determining a value for the latter. The Py/Gr/Cu samples, despite having the same Py properties, showed no change in damping with thickness. This implies a strong suppression of spin flow away from the Py, which we attribute to the large contact resistance at the Gr/Cu interface.

Our results are consistent with the evidence for spin pumping from Py into Gr reported in [13], where an inverse spin Hall voltage was detected at a separate Pd electrode. However, we emphasize that quantitative analysis of spin pumping data requires independent characterization of magnetic properties and a consideration of the effect of all relevant conductances, not only $G_{\uparrow\downarrow}$. Our results are not consistent with the interpretation offered in [30] that Gr itself is a strong spin absorber. We expect that magnetometry and/or a thickness series would show that differences in Py properties, rather than spin pumping, are responsible for the change in damping in this case.

VI. METHODS

A. Cu film deposition and Gr CVD

Epitaxial, crystalline Cu(111) thin films on sapphire were made as described in [33]. In brief, 500 nm of Cu was sputtered onto 50 mm wafers of $\alpha\text{-Al}_2\text{O}_3$ (0001) held at 65°C. During the annealing that preceded Gr growth (see below), secondary grain growth resulted in exclusively Cu(111) grains $\gtrsim 2$ cm across. These large grains prevent dewetting of the Cu film during Gr CVD at higher temperatures [33]. One Cu/ Al_2O_3 wafer was removed after annealing only and used for Py deposition directly on Cu, while a second wafer continued through the Gr growth step.

Gr CVD was performed in a hot-wall quartz tube furnace with a diameter of 76 mm. After evacuating the tube with a dry pump to a pressure of 0.67 Pa (5 mTorr), the rest of the process was performed at a total pressure of 80 kPa (600 Torr). The wafer was heated in a flow of 7 sccm H_2 and 2100 sccm Ar (H_2 partial pressure of 0.3 kPa (2 Torr)), initially ramping to 920°C in about 15 min and then moving to 1000°C at 2°C/min to allow complete Cu grain growth. The temperature was then increased to 1060°C and the gas flows were changed to 58 sccm H_2 and 3600 sccm Ar (H_2 partial pressure of 1.3 kPa (9.5 Torr)). After 10 min under these conditions, Gr growth was initiated by adding 18 sccm of 0.2% CH_4 in Ar (CH_4 partial pressure of 0.8 Pa (6 mTorr)). Growth conditions were maintained for 3 h before rapid cooling by opening the furnace lid. The flow of CH_4 was

stopped below 400°C and the flow of H_2 was stopped below 100°C.

The resulting Gr films were characterized by optical microscopy to check for completeness of growth and Raman spectroscopy to confirm their quality. For shorter growth times, for which Gr coverage was incomplete, we found this growth recipe consistently gave compact hexagonal Gr growth domains with nucleation sites separated by ≈ 100 μm .

Both wafers were cut into 6 mm \times 8 mm chips using a diamond scribe.

B. Py sputter deposition

For each thickness, Py was deposited simultaneously onto bare Cu and Gr/Cu samples. To remove Cu oxide and adventitious contamination, samples were soaked in glacial acetic acid for 1 min and rinsed in deionized water just prior to being placed in the load lock of a deposition chamber with a base pressure $\approx 4 \times 10^{-6}$ Pa (3×10^{-8} Torr). The samples were heated to $\approx 200^\circ\text{C}$ to remove residual water and then cooled in vacuum to $\approx 50^\circ\text{C}$ before deposition. Depositions at both $\theta = 90^\circ$ and $\theta = 30^\circ$ were performed with the source running at 200 W and ≈ 430 V, in 1.1 mTorr of Ar gas, and with a target-to-sample distance of 23 cm. The deposition rates, measured using atomic force microscopy for ≈ 10 nm thick films, were 0.03 nm/s for $\theta = 90^\circ$ and 0.09 nm/s for $\theta = 30^\circ$.

C. Magnetometry

The VSM measurements were performed at room temperature with the sample mounted in a plastic straw, using a frequency of 40 Hz, and an oscillation amplitude of 2 mm. The magnetic field, applied in the plane of the sample, was swept over a range of $\mu_0 H = \pm 4$ T to allow a linear fit to the diamagnetic background, due primarily to the Al_2O_3 substrate. The moment of the Py layer was taken as the $H = 0$ intercept value of a linear fit from 1 T to 4 T.

D. Raman spectroscopy

We performed Raman spectroscopy in a home-built system using a 532 nm diode laser with a power of ≈ 3.5 mW and a spot size < 10 μm . Peak fitting was done after subtracting a smooth fit to the surrounding background from Cu fluorescence.

ACKNOWLEDGMENTS

The authors thank Justin Shaw for valuable comments on interfacial anisotropy in Py, Bill Rippard and

Justin Shaw for help in maintaining the sputter deposition chamber, and Ben Derby for help in sample preparation. Optical microscopy and TEM were done in NIST's Precision Imaging Facility.

AUTHOR CONTRIBUTIONS

MWK, TJS, and WJG designed the experiments. WJG made the Gr/Cu substrates, deposited the Py films, and performed VSM and Raman measurements. HTN performed FMR measurements and TJS performed FMR data analysis. ACD performed TEM sample preparation and imaging. MWK developed the two-angle sputtering method. MWK and WJG wrote the manuscript. All authors contributed to interpretation of the data and commented on the manuscript.

APPENDIX A: MODEL FOR SPIN PUMPING IN MULTI-LAYER STRUCTURES

Following [32], we model the spin transport of a FM layer in contact with one or more NM layers as an electrical circuit of resistors in series. Fig. 7 shows the simplest case of one interfacial resistance, $1/G_{\uparrow\downarrow}$, and one external resistance, $1/G_{\text{ext}}$. The effective conductance for spin current flowing from the FM to the spin sink is simply

$$\frac{1}{G_{\text{eff}}} \equiv \frac{1}{G_{\uparrow\downarrow}} + \frac{1}{G_{\text{ext}}}.$$

Since these conductances describe spin transport perpendicular to the FM/NM interface, they are defined per unit area of the interface and have units of $\Omega^{-1} \cdot \text{m}^{-2}$. In the full theory of spin pumping [1], $G_{\uparrow\downarrow}$ is a complex quantity whose real part affects damping and whose imaginary part affects the FM precession frequency. For conventional FM metals such as Ni, Fe, and Co, the effect on frequency is negligible [34] and $G_{\uparrow\downarrow}$ is commonly used to refer only to the real part.

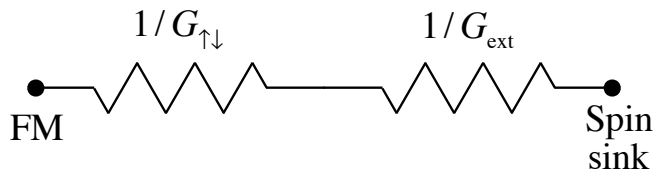


FIG. 7. Series resistor model for spin transport between a FM and a NM spin sink.

The interfacial conductance $G_{\uparrow\downarrow}$, often called the “spin-mixing” conductance, determines how readily spins can move across the FM/NM interface. This process is governed by the exchange interaction, which operates over a length scale of a few nanometers. For metallic interfaces, the theoretical upper bound on $G_{\uparrow\downarrow}$ [7] is the Sharvin conductance [35] (for a single spin direction and

per unit area), corresponding to perfect transmission for every conductance channel at the interface,

$$G_S = \frac{e^2}{h} \frac{k_F^2}{4\pi},$$

where k_F is the Fermi wavevector. Taking Cu as a typical metal, with $k_F = 1.36 \times 10^{10} \text{ m}^{-1}$, we find $G_S \approx 0.5 \times 10^{15} \Omega^{-1} \cdot \text{m}^{-2}$. Both experimental and theoretical results for Py/Cu interfaces (and several other FM/NM combinations) are consistent with this limit [5–9], with $G_{\uparrow\downarrow}$ in the range of $(0.5 \pm 0.1) \times 10^{15} \Omega^{-1} \cdot \text{m}^{-2}$.

The external conductance G_{ext} determines how readily spins flow away from the interface once they have entered the NM material. For a single NM layer of thickness d_{NM} , bulk electrical conductivity σ , and spin diffusion length λ_s , G_{ext} is given in [32] as

$$G_{\text{ext}} = \frac{1}{2} \frac{\sigma}{\lambda_s} \tanh \frac{d_{\text{NM}}}{\lambda_s}.$$

For $d_{\text{NM}} \gtrsim 2\lambda_s$, which is often the case, the external spin conductance is simply determined by the ratio of conductivity and spin diffusion length, $G_{\text{ext}} \approx \sigma/2\lambda_s$.

In the limit of $G_{\text{ext}} \gg G_{\uparrow\downarrow}$, when spins diffuse rapidly away from the interface, $G_{\text{eff}} \approx G_{\uparrow\downarrow}$ and a measurement of $\Delta\alpha_{\text{sp}}$ can be used to directly infer a value of $G_{\uparrow\downarrow}$ from Eq. 1. This limit applies to NM materials with large σ and/or small λ_s , such as Pt and Pd [32]. However, other materials such as Ta and Cu [32] are in the opposite limit, where $G_{\text{eff}} \approx G_{\text{ext}}$ and $\Delta\alpha_{\text{sp}}$ is not sensitive to $G_{\uparrow\downarrow}$.

APPENDIX B: FULL FMR RESULTS

Table II shows all parameters obtained by fitting the FMR data for each sample. These results are plotted in Figs. 8, 9, and 10. Values of g come from fits to Equation 2, where $\gamma = \frac{q\mu_B}{h}$.

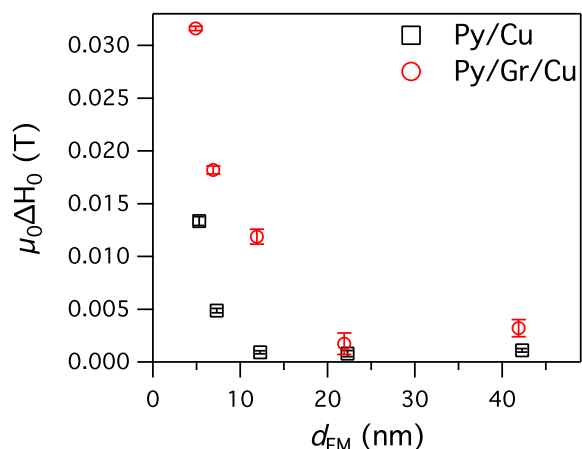
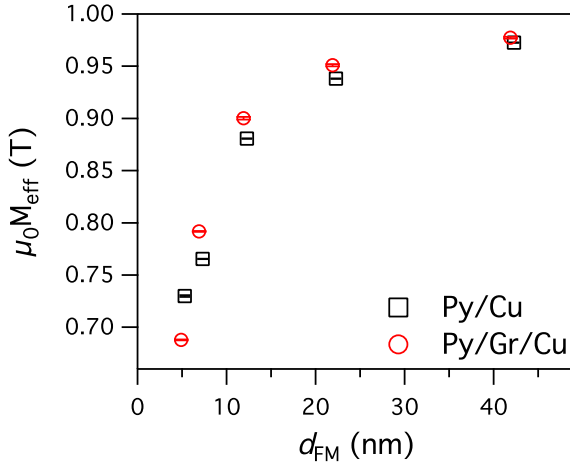
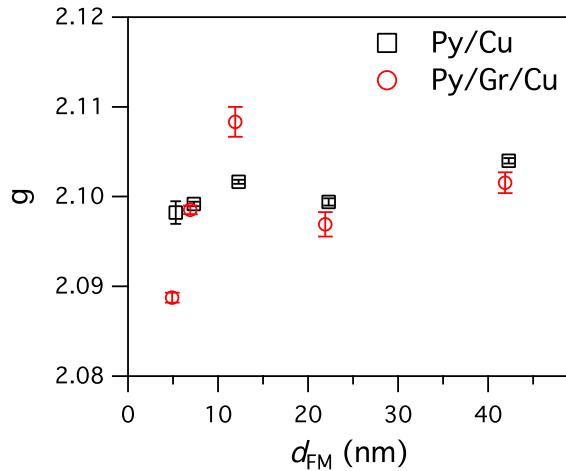


FIG. 8. Plot of ΔH_0 vs Py thickness.

	d_0 (nm)	$\mu_0 M_{\text{eff}}$ (T)	g	$\mu_0 \Delta H_0$ (mT)	α
Cu+Gr	5+3	0.6879	2.089	31.6	0.0073 ± 0.0001
	5+3	0.7918	2.098	18.2	0.0077 ± 0.0002
	5+10	0.9002	2.108	11.9	0.0072 ± 0.0005
	5+20	0.9509	2.097	1.7	0.0084 ± 0.0007
	5+40	0.9772	2.102	3.2	0.0089 ± 0.0005
Cu	5+3	0.7298	2.098	13.4	0.0138 ± 0.0003
	5+5	0.7654	2.099	4.9	0.0089 ± 0.0001
	5+10	0.8807	2.102	0.9	0.0078 ± 0.0001
	5+20	0.9381	2.099	0.8	0.0075 ± 0.0002
	5+40	0.9725	2.104	1.1	0.0076 ± 0.0001

TABLE II. Parameters from FMR fits of $H_{\text{res}}(f)$ and $\Delta H(f)$.FIG. 9. Plot of M_{eff} vs Py thickness.FIG. 10. Plot of g vs Py thickness.

APPENDIX C: GRAPHENE DAMAGE ESTIMATES

Expected Damage Rate from Ar Neutrals

The simulation results in [20] can be applied to our sputtering conditions to estimate the flux of Ar neutrals arriving at the substrate with sufficient energy to damage the Gr. In particular, the results in Fig. 7 of [20] for 400 eV Ar^+ ions hitting a Cu target are a good estimate for our case of 430 eV Ar^+ hitting a $\text{Ni}_{80}\text{Fe}_{20}$ target. The probability of an Ar neutral reflected normal to the target and with sufficient energy to damage Gr is approximately 2×10^{-4} per unit solid angle for each Ar^+ ion that hits the target. Our sputtering source operates at a current of 0.47 A, corresponding to 2.9×10^{18} Ar^+ ions per second. Our 6 mm \times 8 mm substrate, oriented at $\theta = 30^\circ$ and at a distance of 230 mm from the target, subtends a solid angle of 7.9×10^{-4} sr. The result in Fig. 21 of [20] shows that there is negligible scattering of Ar neutrals for our pressure-distance product of 35 Pa \cdot mm. This yields a flux of damaging Ar neutrals at our substrate of about $0.009 \text{ nm}^{-2} \cdot \text{s}^{-1}$, remarkably close to the value of $0.005 \text{ nm}^{-2} \cdot \text{s}^{-1}$ inferred from the Raman spectrum of the 2 s exposure described in the main text.

Raman Measurement of Gr Damage vs. Angle

In order to evaluate Gr damage as a function of sputtering angle, we deposited ≈ 10 nm of Py at several angles between $\theta = 30^\circ$ and $\theta = 90^\circ$ and made Raman measurements. The results for I_D/I_G and I_{2D}/I_G are shown in Fig. 11.

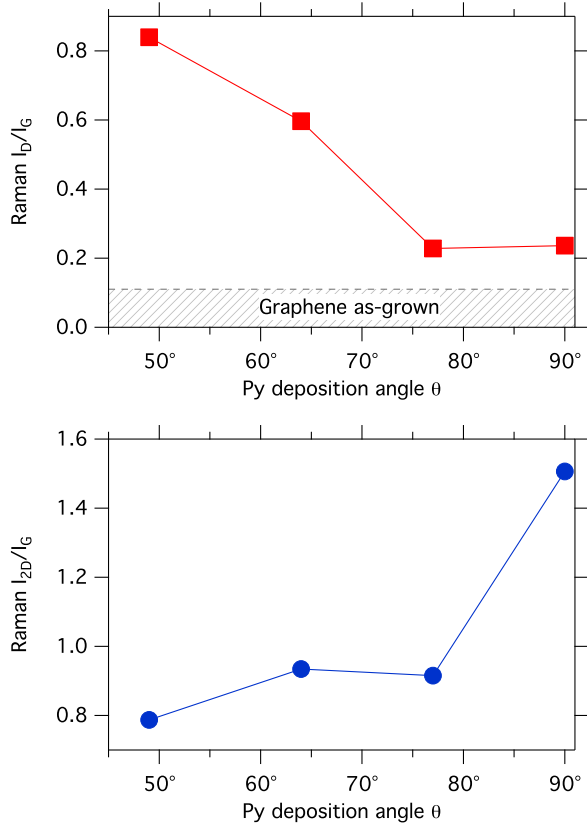


FIG. 11. Raman peak ratios I_D/I_G and I_{2D}/I_G vs Py angle of incidence θ .

-
- [1] A. Brataas and K. M. D. Hals, *Nature Nano.*, **9**, 86 (2014).
 - [2] D. C. Ralph and M. D. Stiles, *J. Magn. Magn. Mater.*, **320**, 1190 (2008).
 - [3] K. Ando, S. Fujita, J. Ito, S. Yuasa, Y. Suzuki, Y. Nakatani, T. Miyazaki, and H. Yoda, *J. Appl. Phys.*, **115**, 172607 (2014).
 - [4] Y. Tserkovnyak, A. Brataas, and G. E. W. Bauer, *Phys. Rev. Lett.*, **88**, 117601 (2002).
 - [5] Y. Tserkovnyak, A. Brataas, and G. E. W. Bauer, *Phys. Rev. B*, **66**, 224403 (2002).
 - [6] K. Xia, P. J. Kelly, G. E. W. Bauer, A. Brataas, and I. Turek, *Phys. Rev. B*, **65**, 220401 (2002).
 - [7] G. E. W. Bauer, Y. Tserkovnyak, D. Huertas-Hernando, and A. Brataas, *Phys. Rev. B*, **67**, 094421 (2003).
 - [8] T. Gerrits, M. L. Schneider, and T. J. Silva, *J. Appl. Phys.*, **99**, 023901 (2006).
 - [9] J. M. Shaw, H. T. Nembach, and T. J. Silva, *Phys. Rev. B*, **85**, 054412 (2012).
 - [10] S. Mizukami, Y. Ando, and T. Miyazaki, *J. Magn. Magn. Mater.*, **226–230**, 1640 (2001).
 - [11] S. Mizukami, Y. Ando, and T. Miyazaki, *Jap. J. Appl. Phys.*, **40**, 580 (2001).
 - [12] W. Han, K. McCreary, K. Pi, W. Wang, Y. Li, H. Wen, J. Chen, and R. Kawakami, *J. Magn. Magn. Mater.*, **324**, 369 (2012).
 - [13] Z. Tang, E. Shikoh, H. Ago, K. Kawahara, Y. Ando, T. Shinjo, and M. Shiraishi, *Phys. Rev. B*, **87**, 140401 (2013).
 - [14] S. Singh, A. Ahmadi, C. T. Cherian, E. R. Mucciolo, E. del Barco, and B. Özyilmaz, *Appl. Phys. Lett.*, **106**, 032411 (2015).
 - [15] A. J. Berger, W. Amamou, S. P. White, R. Adur, Y. Pu, R. K. Kawakami, and P. C. Hammel, *J. Appl. Phys.*, **115**, 17C510 (2014).
 - [16] J. A. Robinson, M. LaBella, M. Zhu, M. Hollander, R. Kasarda, Z. Hughes, K. Trumbull, R. Cavaleiro, and D. Snyder, *Appl. Phys. Lett.*, **98**, 053103 (2011).
 - [17] R. McMichael and P. Krivosik, *IEEE Trans. Magn.*, **40**, 2 (2004).
 - [18] H. T. Nembach, T. J. Silva, J. M. Shaw, M. L. Schneider, M. J. Carey, S. Maat, and J. R. Childress, *Phys. Rev. B*, **84**, 054424 (2011).
 - [19] C.-T. Chen, E. A. Casu, M. Gajek, and S. Raoux, *Appl. Phys. Lett.*, **103**, 033109 (2013).

- [20] Y. Yamamura and M. Ishida, *J. Vac. Sci. Technol. A*, **13**, 101 (1995).
- [21] O. Lehtinen, J. Kotakoski, A. V. Krashennnikov, A. Tolvanen, K. Nordlund, and J. Keinonen, *Phys. Rev. B*, **81**, 153401 (2010).
- [22] O. Lehtinen, J. Kotakoski, A. V. Krashennnikov, and J. Keinonen, *Nanotechnology*, **22**, 175306 (2011).
- [23] A. C. Ferrari and D. M. Basko, *Nature Nano.*, **8**, 235 (2013).
- [24] L. G. Cançado, A. Jorio, E. H. M. Ferreira, F. Stavale, C. A. Achete, R. B. Capaz, M. V. O. Moutinho, A. Lombardo, T. S. Kulmala, and A. C. Ferrari, *Nano Lett.*, **11**, 3190 (2011).
- [25] J. F. Ziegler, M. Ziegler, and J. Biersack, *Nuclear Instrum. Meth. Phys. B*, **268**, 1818 (2010).
- [26] J. O. Rantschler, P. J. Chen, A. S. Arrott, R. D. McMichael, W. F. Egelhoff, and B. B. Maranville, *J. Appl. Phys.*, **97**, 10J113 (2005).
- [27] G. C. Bailey and C. Vittoria, *Phys. Rev. B*, **8**, 3247 (1973).
- [28] K. Rook, A. M. Zeltser, J. O. Artman, D. E. Laughlin, M. H. Kryder, and R. M. Chrenko, *J. Appl. Phys.*, **69**, 5670 (1991).
- [29] L. A. Giannuzzi, J. L. Drown, S. R. Brown, R. B. Irwin, and F. A. Stevie, *MRS Proceedings*, **480**, 19 (1997).
- [30] A. K. Patra, S. Singh, B. Barin, Y. Lee, J.-H. Ahn, E. del Barco, E. R. Mucciolo, and B. Özyilmaz, *Appl. Phys. Lett.*, **101**, 162407 (2012).
- [31] J. Bass and W. P. Pratt, *J. Phys. Condens. Matter*, **19**, 183201 (2007).
- [32] C. T. Boone, H. T. Nembach, J. M. Shaw, and T. J. Silva, *J. Appl. Phys.*, **113**, 153906 (2013).
- [33] D. L. Miller, M. W. Keller, J. M. Shaw, K. P. Rice, R. R. Keller, and K. M. Diederichsen, *AIP Advances*, **3**, 082105 (2013).
- [34] M. Zwierzycki, Y. Tserkovnyak, P. J. Kelly, A. Brataas, and G. E. W. Bauer, *Phys. Rev. B*, **71**, 064420 (2005).
- [35] Y. V. Sharvin, *Sov. Phys. JETP*, **21**, 655 (1965).